Fig. 3

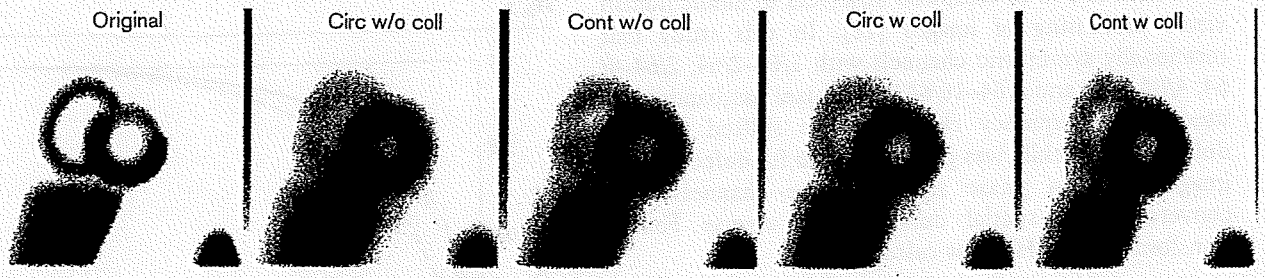

Example reconstructed short-axis slices obtained with circular and body-contour orbit with/without collimator response compensation (coll). Original image has enhanced defect contrast.

explained in Introduction. We proposed that collimator response modelling might reduce these artefacts and could therefore offer better image quality. No significant acquisition orbit related artefacts were, however, noticed in this study. The absence of artefacts might be partly related to the utilization of 360° acquisitions orbits, which have shown to be less prone to errors than 180° orbits [1]. Moreover, many of the studies that have reported artefacts with body-contour orbits have used filtered back-projection (FBP) as reconstruction method, whereas we used OSEM, which is known to provide images with higher quality than FBP. Even though the body-contour orbit and collimator response compensation combination did not outperform circular orbit with collimator response correction, the collimator response compensation itself was noticed to be very valuable. Collimator response correction increased AUC by 0.045 for circular and by 0.032 for body-contour orbit. Both improvements were statistically significant. Similar findings have been presented before [23,24].

This study has three primary limitations, which are discussed next. First the acquisition orbit comparison was performed using simulated rather than real patient data and thus might not provide the level of realism of a clinical study. On the other hand the complete lack of patient motion and other such factors that deteriorate the quality of clinical SPECT studies allowed us to concentrate only to differences due to acquisition orbits. Moreover, the exact knowledge of the size, shape and location of the defects made the detection performance measurements reliable. This investigation would have been quite difficult to perform as a clinical study: In order to obtain statistically reliable results a large patient population with, for example, angiography information would have been needed. Each patient participating in the study would have also needed two sequential SPECT scans, which would have increased patient discomfort and risk for motion artefacts, in addition to halving the throughput of our scanner.

Second, the simulations in this study were performed using an analytical projection code instead of a Monte Carlo simulator. An analytical simulator was chosen because many of the Monte Carlo packages available do not directly support acquisitions with non-symmetrical body-contour orbits. Our analytical simulator, on the other hand, allows easy modelling of the acquisition orbit. The collimator response modelling in our simulator is performed using similar method as with the popular SIMIND [25] and SIMSET [26] Monte Carlo packages. Thus the only larger difference between our analytical and Monte Carlo simulators is the incorporation of scatter. Scatter modelling in our simulator was implemented using Hutton's method and although this method produces relatively crude scatter approximation it still increases the realism of the projection data. We also believe that accurate scatter modelling is not so important in this study, because we are studying resolution effects.

Third, the image quality was assessed using computer observer instead of human observers. We chose computer observers, because human observer studies are time-consuming and expensive to perform. The CHO used in this work has, however, shown to correlate well with human observers [9,27]. CHOs can also provide much better prediction of human performance than metrics like resolution, contrast and noise level, which are often used to compare acquisition and reconstruction methods.

In conclusion, circular and body-contour orbits offer quite similar defect detection performance and thus the selection of acquisition orbit is of not vital importance in cardiac SPECT. Collimator response compensation, on the other hand, significantly increases defect detectability regardless of acquisition type and should therefore be applied in reconstruction whenever available.

Acknowledgement

This work was supported by grants from Japan Society for the Promotion of Science.

References

1 Eisner RL, Nowak DJ, Pettigrew R, Fajman W. Fundamentals of 180° acquisition and reconstruction in SPECT imaging. *J Nucl Med* 1986; 27:1717–1728.

2 O'Connor MK, Hruska CB. Effect of tomographic orbit and type of rotation on apparent myocardial activity. *Nucl Med Commun* 2005; 26:25–30.

3 Maniawski PJ, Morgan HT, Wackers FJT. Orbit-related variation in spatial resolution as a source of artifactual defects in thallium-201 SPECT. *J Nucl Med* 1991; 32:871–875.

4 Abufadel A, Eisner RL, Schafer RW. Differences due to collimator blurring in cardiac images with use of circular and elliptic camera orbits. *J Nucl Cardiol* 2001; 8:458–465.

5 Hutton BF, Lau YH. Application of distance-dependent resolution compensation and post-reconstruction filtering for myocardial SPECT. *Phys Med Biol* 1998; 43:1679–1693.

6 Lau YH, Hutton BF, Beekman FJ. Choice of collimator for cardiac SPET when resolution compensation is included in iterative reconstruction. *Eur J Nucl Med* 2001; 28:39–47.

7 Zeng GL, Gullberg GT. Frequency domain implementation of the three-dimensional geometric point response correction in SPECT imaging. *IEEE Trans Nucl Sci* 1992; 39:1444–1453.

8 Zeng GL, Gullberg GT, Bai C, Christian PE, Trisjono F, Di Bella EVR, *et al.* Iterative reconstruction of fluorine-18 SPECT using geometric point response correction. *J Nucl Med* 1998; 39:124–130.

9 Wollenweber SD, Tsui BMW, Lalush DS, Frey EC, LaCroix KJ, Gullberg GT. Comparison of Hotelling observer models and human observers in defect detection from myocardial SPECT imaging. *IEEE Trans Nucl Sci* 1999; 46:2098–2103.

10 Tsui BMW, Zhao XD, Gregoriou GK, Lalush DS, Frey EC, Johnston RE, *et al.* Quantitative cardiac SPECT reconstruction with reduced image degradation due to patient anatomy. *IEEE Trans Nucl Med* 1994; 41:2838–2844.

11 Pretorius PH, King MA, Tsui BMW, LaCroix KJ, Xia W. A mathematical model of motion of the heart for use in generating source and attenuation maps for simulating emission imaging. *Med Phys* 1999; 26:2323–2332.

12 Metz CE, Atkins FB, Beck RN. The geometric transfer function component for scintillation camera collimators with straight parallel holes. *Phys Med Biol* 1980; 25:1059–1070.

13 Frey EC, Tsui BMW, Gullberg GT. Improved estimation of the detector response function for converging beam collimators. *Phys Med Biol* 1998; 43:941–950.

14 Hutton BF, Osiecki A, Meikle SR. Transmission-based scatter correction of 180° myocardial single-photon emission tomographic studies. *Eur J Nucl Med* 1996; 23:1300–1308.

15 Hutton BF, Baccarne V. Efficient scatter modelling for incorporation in maximum likelihood reconstruction. *Eur J Nucl Med* 1998; 25:1658–1665.

16 Hudson HM, Larkin RS. Accelerated image reconstruction using ordered subsets of projection data. *IEEE Trans Med Imag* 1994; 13:601–609.

17 Di Bella EVR, Barclay AB, Eisner RL, Schafer RW. A comparison of rotation-based methods for iterative reconstruction algorithms. *IEEE Trans Nucl Sci* 1996; 43:3370–3376.

18 Frey EC, Gilland KL, Tsui BMW. Application of task-based measures of image quality to optimization and evaluation of three-dimensional reconstruction-based compensation methods in myocardial perfusion SPECT. *IEEE Trans Med Imag* 2002; 21:1040–1050.

19 Narayanan MV, Gifford HC, King MA, Pretorius PH, Famcombe TH, Bruyant P, *et al.* Optimization of iterative reconstructions of ^{99m}Tc cardiac SPECT studies using numerical observers. *IEEE Trans Nucl Sci* 2002; 5:2355–2360.

20 Myers KJ, Barrett HH. Addition of a channel mechanism to the ideal-observer model. *J Opt Soc Am A* 1987; 4:2447–2457.

21 Shidahara M, Inoue K, Maruyama M, Watabe H, Taki Y, Goto R, *et al.* Predicting human performance by channelized Hotelling observer in discriminating between Alzheimer's dementia and controls using statistically processed brain perfusion SPECT. *Ann Nucl Med* 2006; 20:605–613.

22 White MP, Russell A, Mascitelli VA, Morris RS, Shehata AR, Heller GV. Clinical comparison of circular versus noncircular acquisition using technetium-99m myocardial perfusion SPECT imaging. *J Nucl Med Technol* 1997; 25:37–40.

23 He X, Links JM, Gilland GL, Tsui BMW, Frey EC. Comparison of 180° and 360° acquisition for myocardial perfusion SPECT with compensation for attenuation, detector response, and scatter: Monte Carlo and mathematical observer results. *J Nucl Cardiol* 2006; 13:345–353.

24 Narayanan MV, King MA, Pretorius PH, Dahlberg ST, Spencer F, Simon E, *et al.* Human-observer receiver-operating-characteristic evaluation of attenuation, scatter, and resolution compensation strategies for ^{99m}Tc myocardial perfusion imaging. *J Nucl Med* 2003; 44:1725–1734.

25 Ljungberg M, Strand S-E. A Monte Carlo program for the simulation of scintillation camera characteristics. *Comput Methods Programs Biomed* 1989; 29:257–272.

26 Harrison RL, Vannoy SD, Haynor DR, Gillispie SB, Kaplan MS, Lewellen TK. Preliminary experience with the photon history generator module of a public-domain simulation system for emission tomography. *Conf Rec IEEE Nucl Sci Symp* 1993; 1154–1158.

27 Sankaran S, Frey EC, Gilland KL, Tsui BMW. Optimum compensation method and filter cutoff frequency in myocardial SPECT: a human observer study. *J Nucl Med* 2002; 43:432–438.

Ann Nucl Med (2007) 21:537–543
DOI 10.1007/s12149-007-0057-4

TECHNICAL NOTE

Accelerated 3D-OSEM image reconstruction using a Beowulf PC cluster for pinhole SPECT

Tsutomu Zeniya · Hiroshi Watabe · Antti Sohlberg
Hidehiro Iida

Received: 18 May 2007 / Accepted: 6 August 2007

Abstract
Objective A conventional pinhole single-photon emission computed tomography (SPECT) with a single circular orbit has limitations associated with non-uniform spatial resolution or axial blurring. Recently, we demonstrated that three-dimensional (3D) images with uniform spatial resolution and no blurring can be obtained by complete data acquired using two-circular orbit, combined with the 3D ordered subsets expectation maximization (OSEM) reconstruction method. However, a long computation time is required to obtain the reconstruction image, because of the fact that 3D-OSEM is an iterative method and two-orbit acquisition doubles the size of the projection data. To reduce the long reconstruction time, we parallelized the two-orbit pinhole 3D-OSEM reconstruction process by using a Beowulf personal computer (PC) cluster.
Methods The Beowulf PC cluster consists of seven PCs connected to Gbit Ethernet switches. Message passing interface protocol was utilized for parallelizing the reconstruction process. The projection data in a subset are distributed to each PC. The partial image forward- and back-projected in each PC is transferred to all PCs. The current image estimate on each PC is updated after summing the partial images. The performance of parallelization on the PC cluster was evaluated using two independent projection data sets acquired by a pinhole SPECT system with two different circular orbits.
Results Parallelization using the PC cluster improved the reconstruction time with increasing number of PCs. The reconstruction time of 54 min by the single PC was decreased to 10 min when six or seven PCs were used. The speed-up factor was 5.4. The reconstruction image by the PC cluster was virtually identical with that by the single PC.
Conclusions Parallelization of 3D-OSEM reconstruction for pinhole SPECT using the PC cluster can significantly reduce the computation time, whereas its implementation is simple and inexpensive.

Keywords Pinhole SPECT · Image reconstruction · 3D-OSEM · PC cluster · Parallel computing

T. Zeniya (✉) · H. Watabe · A. Sohlberg · H. Iida
Department of Investigative Radiology, Advanced Medical Engineering Center, National Cardiovascular Center Research Institute, 5-7-1 Fujishiro-dai, Suita 565-8565, Japan
e-mail: zeniya@ri.ncvc.go.jp

Introduction

Small animal single-photon emission computed tomography (SPECT) allows in vivo high-resolution three-dimensional (3D) imaging of physiological functions in small animals. This facilitates an objective assessment of the pharmaceutical development and regenerative therapy in pre-clinical studies [1–8]. However, a conventional pinhole SPECT with single circular orbit has major limitations associated with non-uniform spatial resolution or axial blurring [1, 9]. This blurring can be moderated by applying statistical image reconstruction methods such as maximum likelihood expectation maximization (MLEM) [10] or ordered subsets expectation maximization (OSEM) [11] rather than Feldkamp's filtered back-projection (Feldkamp-FBP) method [12], but still remains problematic at the periphery of field of view [1, 9]. Recently, we have demonstrated that the uniformity of spatial resolution can be improved by complete projection data acquired with two different circular orbits [13, 14] that satisfy data completeness condition

of Tuy [15], combined with 3D-OSEM. However, a long computation time is required to obtain the reconstructed image because 3D-OSEM is an iterative method and two-circular orbit acquisition doubles the size of the projection data. To reduce the long reconstruction time, we parallelized the two-orbit 3D-OSEM reconstruction process by using a personal computer (PC) cluster. Several investigators have demonstrated speed-up of 3D-OSEM reconstruction in positron emission tomography (PET) [16–19] and SPECT [20]. This study was aimed at improving the speed of the computing time for two-orbit pinhole 3D-OSEM reconstruction. We have previously succeeded in improving the performance of motion correction for PET using a Beowulf PC cluster [21]. Beowulf PC cluster (http://www.beowulf.org) is defined as a cluster of several PCs running a free-software operating system such as Linux or FreeBSD, interconnected by an Ethernet or Myrinet network. Therefore, this cluster system can be extremely inexpensively built compared with conventional super computer systems. In this study, we implemented two-orbit pinhole 3D-OSEM on our Beowulf PC cluster. To test the performance of the PC cluster, actual data were processed and compared with results obtained by a single PC.

Materials and methods

PC cluster

The Beowulf-type PC cluster consists of seven PCs. There are four 2.4 GHz Xeon processors for a master PC and dual 1.4 GHz Pentium III processors for six slave PCs connected to Gbit Ethernet switches (Fig. 1, Table 1). Each PC has 1 GB physical memory. For the parallelizing task, we installed the local area multicomputing (LAM) 6.5.7 version of the message passing interface (MPI) protocol (http://www.lam-mpi.org) on each PC.

Table 1 Specification of our Beowulf personal computer (PC) cluster

Component	Specification
Master PC	PowerEdge 2650 (Dell) 4 Xeon (Intel) 2.4 GHz 1 GB physical memory Linux 2.4.18 operating system
Slave PCs (six)	PowerEdge 1650 (Dell) Dual Pentium III (Intel) 1.4 GHz 1 GB physical memory Linux 2.4.18 operating system
Switching hub	SuperStack 3 Switch 4900 (3COM) 12 × 1000BASE-T port

The program for this system was written in the C language (gcc version 2.96) on a Linux operating system (version 2.4.18).

Theory of formulation for parallelizing two-orbit pinhole 3D-OSEM reconstruction

Figure 2 shows a schematic diagram of two-orbit pinhole SPECT geometry and two-orbit 3D-MLEM iterative reconstruction. The two-orbit 3D-MLEM update can be expressed as

$$\lambda_j^{k+1} = \frac{\lambda_j^k}{\sum_{l=1}^{2}\sum_{i=1}^{n} C_{lij}} \sum_{l=1}^{2}\sum_{i=1}^{n} \frac{y_{li} C_{lij}}{\sum_{j=1}^{m} C_{lij}\lambda_j^k}, \quad (1)$$

where λ_j^k is the value of the image voxel j for the kth iteration, y_{li} is the measured value of the projection pixel i for the lth orbit, and C_{lij} is the probability of detecting a photon originating from image voxel j at projection pixel i for the lth orbit. Each iteration of the MLEM algorithm for two orbits consists of the following four steps: (1) forward-projecting current image estimate λ_j^k for two orbits (forward-projection), (2) dividing the measured and forward projections for two orbits (correction), (3) back-projecting corrections for two orbits (back-projection), and (4) generating λ_j^{k+1} with the back-projected image. A 3D voxel-driven projector using bilinear interpolation on the detector plane was employed in both the back- and forward-projections.

The ordered subsets (OS) scheme was used to reduce the number of iterations, and subsets were evenly divided for both orbits. In our earlier studies [13, 14], as 120

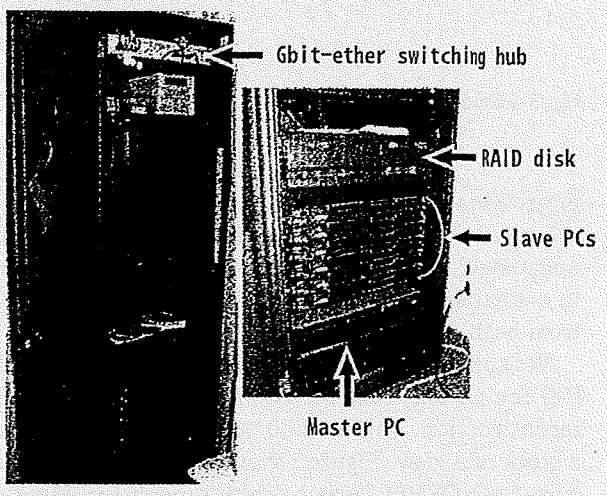

Fig. 1 Photograph of our Beowulf personal computer (PC) cluster

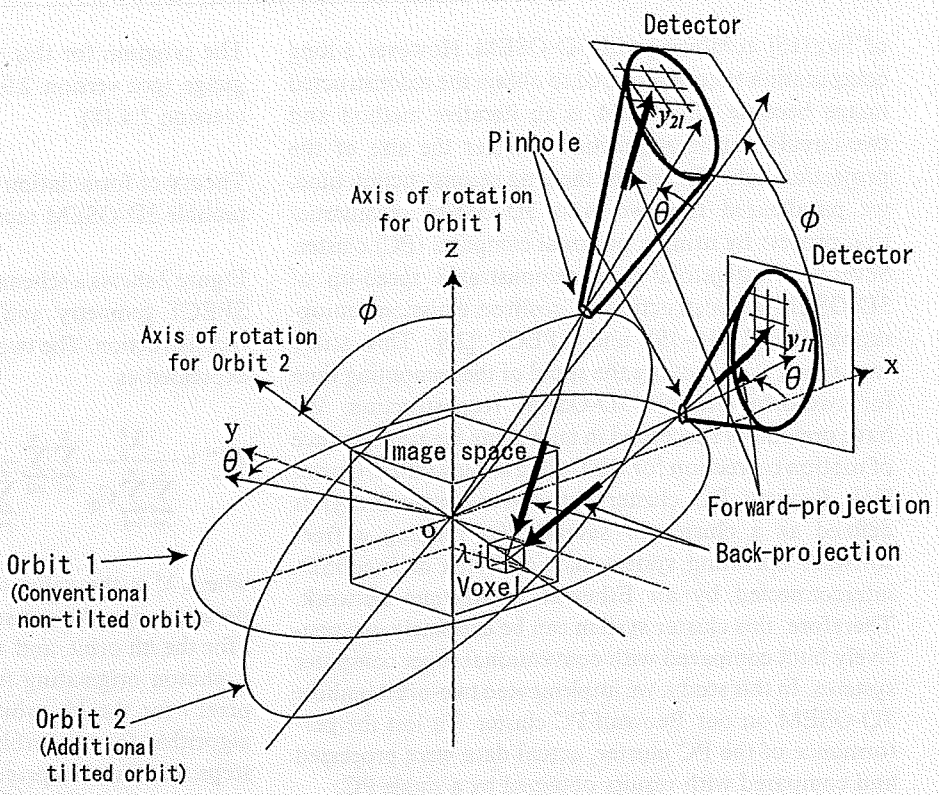

Fig. 2 Schematic diagram of geometry and three-dimensional ordered subsets expectation maximization (3D-OSEM) iterative image reconstruction in the pinhole single-photon emission computed tomography system with two-circular orbit

```
for all Iterations {
    for all Subsets{
        for (Views/Subsets) × Orbits on each PC {        Process 1: in parallel
            Forward-project current image estimate
            Calculate correction (measured projection / forward projection)
            Back-project correction
        }
        Sum partial back-projeced images on all PCs      Process 2: synchronization
        Update current image estimate (image ← image × backprojected image)
    }
}
```

Fig. 3 Pseudocode of parallelized 3D-OSEM for two orbits

projections for single orbit or 240 projections for two orbits were acquired and the current image estimate was updated with 8 subsets, 15 or 30 projections were assigned to one subset (i.e., data of $\theta = 0°, 24°, 48°, 72°, \ldots, 336°$ from both orbits were used to form the first subset).

We applied the projection space decomposition (PSD) [18] for parallelizing the two-orbit pinhole 3D-OSEM reconstruction. This method operates projection data in a block of a view. Figure 3 shows a pseudocode of parallelized 3D-OSEM for two orbits. Process 1 in Fig. 3 can be parallelized because the forward- and back-projection

Table 2 Distribution of 30-projection data in first subset to seven-PC cluster

PC number	Projection number (orbit number)				
1	1 (1)	57 (1)	113 (1)	49 (2)	105 (2)
2	9 (1)	65 (1)	1 (2)	57 (2)	113 (2)
3	17 (1)	73 (1)	9 (2)	65 (2)	
4	25 (1)	81 (1)	17 (2)	73 (2)	
5	33 (1)	89 (1)	25 (2)	81 (2)	
6	41 (1)	97 (1)	33 (2)	89 (2)	
7	49 (1)	105 (1)	41 (2)	97 (2)	

operations associated with each view are independent and can therefore proceed in parallel. At the end of each subset, a partial back-projected image is generated on each PC and these partial images are transferred to all PCs and then summed, to obtain the complete back-projected image (Process 2 in Fig. 3). Image synchronization is required for Process 2. Initial image estimates are loaded on memory on all PCs. The MPI library was used to implement this parallelization. In the MPI protocol, an identical program runs on independent PCs, with their interactions controlled by exchanging messages.

Figure 4 shows the distribution of 15 projections in one subset for single orbit in the case of total 120 projections. Table 2 shows the distribution of 30 projections in the subset for two orbits when seven PCs are used. As

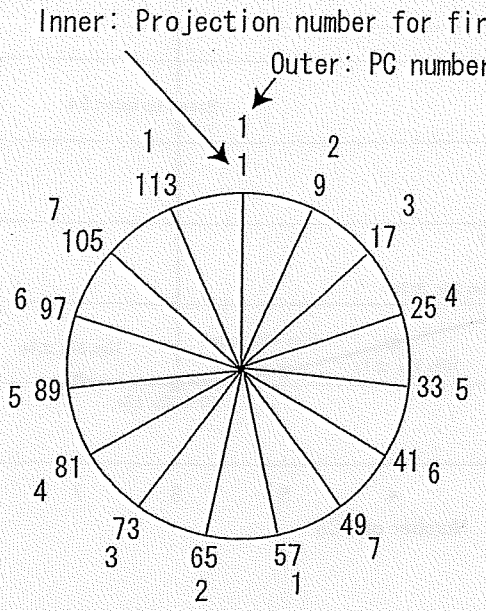

Fig. 4 Distribution of 15-projection data in the first subset for single orbit to seven-PC cluster

shown in Table 2, one PC needs to compute all 30 projections by itself, whereas with seven PC cluster each node uses five projections.

Performance evaluation using pinhole SPECT data

To evaluate the effects of parallelization, data obtained from previous phantom study were used. Detailed descriptions of the pinhole SPECT system were reported previously [13, 14]. This system consisted of a rotating object stage, a fixed conventional SPECT gamma camera (GCA-7100A, Toshiba, Tokyo, Japan) equipped with a pinhole collimator. The system can acquire two independent projection data sets with two different circular orbits to satisfy the completeness condition of Tuy. The rotating stage held the object vertically at tilted angles of $\phi = 0°$ and 45° to satisfy Tuy's condition. A multiple-disk phantom with ^{99m}Tc solution was used to evaluate axial blurring and resolution uniformity [13]. Projection data were acquired for 120 angular views in 3° steps for both orbits, in a 128 × 128 matrix with 16-bit integers. After decay correction, the total size of 240-projection data for two orbits with 32-bit floating point numbers was 15.7 MB. The projection data were reconstructed with eight subsets and two iterations, in a 128 × 128 × 128 matrix with 32-bit floating point numbers (8.4 MB).

Time for reconstruction was measured using different numbers of PCs from one to seven to evaluate the performance of the PC cluster. These measurements were repeated 10 times and the averaged reconstruction time was computed. For reference, the reconstruction time by non-iterative single-orbit Feldkamp-FBP approach was also measured. Feldkamp-FBP program provided by Toshiba was used in this study. The images reconstructed by the PC cluster and single PC were compared to verify whether they equaled. The difference of the two images was evaluated voxel by voxel by calculating the reconstruction error as

$$\varepsilon = \max_j \frac{|\lambda_j^S - \lambda_j^M|}{\lambda_j^S} \times 100(\%), \quad (2)$$

where λ_j^S is the voxel value of image obtained with single PC and λ_j^M obtained by PC cluster.

Results

Figure 5 shows the relationship between the number of PCs and the reconstruction time. The reconstruction time was reduced by increasing the number of PCs. The reconstruction time was 54 min and 18 s with a single PC, and was reduced to 10 min and 2 s with PC cluster. The speed-up factor was approximately 5.4. In this study, the reconstruction time with seven PCs was not improved compared with that with six PCs. The reconstruction time using single-orbit Feldkamp-FBP was 2 min and 44 s. The long reconstruction time by our two-orbit 3D-OSEM was greatly reduced by parallelization with PC cluster, and compared with Feldkamp-FBP, the computation time was about 7 min longer with the PC cluster whereas it was about 52 min longer with the single PC.

As shown in Fig. 6, the image reconstructed by the cluster with six PCs was virtually identical with that with the single PC, and considerably better than image by the single-orbit Feldkamp-FBP method. The reconstruction error ε for the difference between these two images was 0.0001% from Eq. 2.

Discussion

We recently demonstrated that the major limitations in conventional pinhole SPECT, namely, non-uniform spatial resolution or axial blurring in reconstruction images were dramatically improved by complete data acquired using two circular orbits, combined with 3D-OSEM iterative reconstruction. One of the drawbacks of this approach is that it takes a long time to reconstruct in compensation for excellent image from two

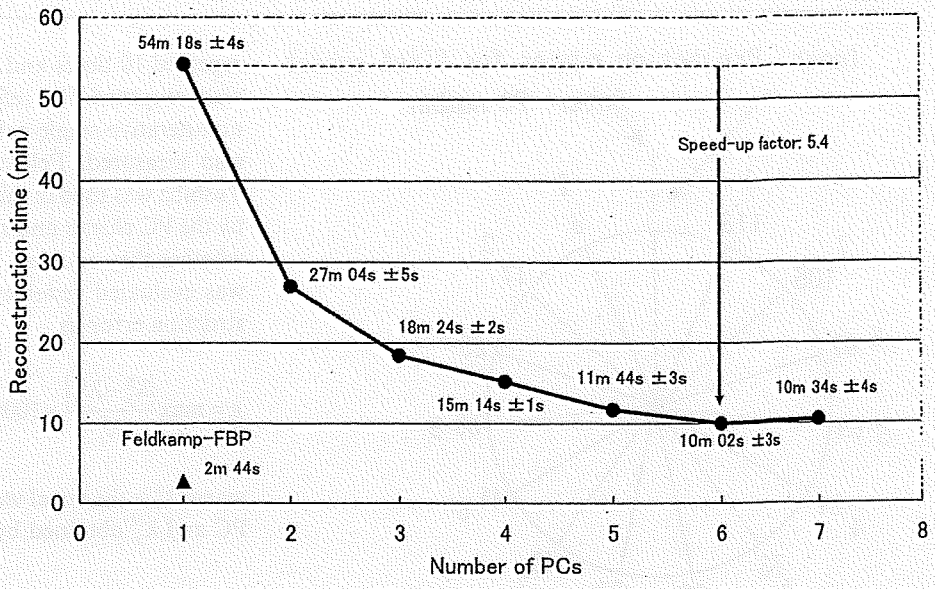

Fig. 5 Relationship between the number of PCs and reconstruction time (min) in parallel computing using the PC cluster

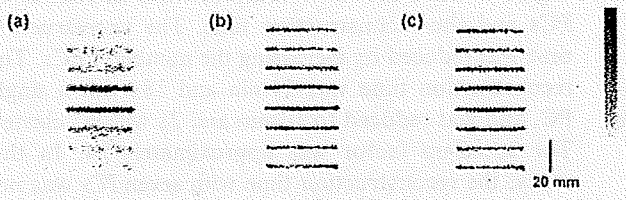

Fig. 6 Coronal images of the multiple-disk phantom reconstructed. The image (a) was reconstructed by the single-orbit Feldkamp-filtered back-projection method on single PC. The image (b) was reconstructed by the two-orbit 3D-OSEM method on single PC. The image (c) was reconstructed by the two-orbit 3D-OSEM method with PC cluster (six PCs)

independent projection data sets with two circular orbits. In this study, the long reconstruction time could be markedly reduced by parallel computing with the PC cluster. The parallelized reconstruction could be needed when resolution recovery, attenuation correction, and scatter correction are used in pinhole SPECT because they also increase the computation time [22].

The image reconstructed using the PC cluster was compared with that using the single PC. The error ε for evaluating the difference between these two images was 0.0001%, meaning that they were virtually identical. This slight error is attributed to the fact that the order of the addition of data back-projected from each view in the PC cluster is different from that in the single PC, and might have occurred during computation of the partial back-projection. However, this difference is negligible as shown by the small value of ε.

In this study, the reconstruction time with seven PCs was not improved compared with that with six PCs, as shown in Fig. 5, because the number of projections processed per one PC in the case of both six and seven PCs were equal. The partial back-projected images on each PC have to be transferred to all PCs, to sum those images on all PCs as shown in Process 2 in Fig. 3. Therefore, the communication time using seven PCs was longer than that using six PCs. The network performance is important for the Beowulf PC cluster.

This study was performed using the cluster with seven PCs. If the cluster had 30 PCs, one PC would process for only one projection. Assuming a linear model and roughly estimating from the results of this study, the reconstruction time using 30 PCs will equal that of 2–3 min with single-orbit FBP. Practically linear speed-up is not expected because back-projection is not a complete parallel process. The partial back-projected images on all PCs have to be transferred to all PCs and then summed on each PC with synchronization. We should consider that the communication time to transfer the partial images increases with increasing the number of PCs or enlarging the size of data. A high-performance communication network is essential for such cases [19]. When the size of the data is large, sufficient physical memory should be prepared to avoid memory swapping which increases the computation time.

To further improve the PC cluster, we must consider optimizing the use of each PC. In this study, there is an imbalance of the load distribution when using seven PCs. As shown in Table 2, while PC 1 and PC 2 process

for the fifth projections of the projections distributed, the other PCs are idle. If projections processed are more evenly distributed to all PCs, the speed of computation should be improved further. The reason for such a non-uniform distribution in this system is that one detector space cannot be decomposited in the combination of voxel-driven projector and PSD. There are two approaches available to evenly distribute data for all the PCs: (i) apply a ray-driven projector [23] instead of voxel-driven one for PSD because it allows the decomposition of one detector space and (ii) apply the image space decomposition method [18] for voxel-driven projector. However, further investigations are required to confirm that these alternative approaches improve the computation speed. When the cluster has slow PCs or other tasks use the resources in the cluster, the reconstruction time will increase as a result of spending too much time on slow PCs. In the present system, the fast PCs wait until the slow PCs complete the back-projection process. If the cluster system monitors the computation speed and the progress of the process on each PC and manages the distribution of the process to idle or fast PCs, the speed-down of reconstruction will be avoided [16].

At present we do not parallelize for one PC with multiple processors. Because the multiple processors on one PC can share memory, communication through the network for summing partial images is unnecessary [16]. Shattuck et al. [17] reported that a four-processor computer was able to achieve speed-up factors of approximately 3.4 relative to a single processor. Parallelization for both cluster PCs and multiple processors will effectively speed up the reconstruction time.

The Beowulf PC cluster system can be constructed using essentially free-software such as Linux operating system and MPI, and inexpensive PCs instead of super computer. Also, modifications of only approximately 10 lines were required to parallelize the reconstruction program. Although this article describes parallelization for the two-orbit pinhole SPECT, the strategy can be generalized for any pinhole SPECT (e.g., single orbit, helical orbit, and multipinholes).

Conclusions

We were able to markedly improve the long computation time of 3D-OSEM reconstruction in two-circular orbit pinhole SPECT by parallel computing using the PC cluster. The reconstruction time of 54 min decreased to 10 min by using six PCs. The speed-up factor was 5.4. The PC cluster is effective in decreasing the computing time with low cost and easy construction.

Acknowledgment This study was partly supported by the Japan Science and Technology Agency (JST).

References

1. Jaszczak RJ, Li J, Wang H, Zalutsky MR, Coleman RE. Pinhole collimation for ultra-high-resolution, small-field-of-view SPECT. Phys Med Biol 1994;39:425–37.
2. Weber DA, Ivanovic M, Franceschi D, Strand SE, Erlandsson K, Franceschi M, et al. Pinhole SPECT: an approach to in vivo high resolution SPECT imaging in small laboratory animals. J Nucl Med 1994;35:342–8.
3. Ishizu K, Mukai T, Yonekura Y, Pagani M, Fujita T, Magata Y, et al. Ultra-high resolution SPECT system using four pinhole collimators for small animal studies. J Nucl Med 1995;36:2282–7.
4. Ogawa K, Kawade T, Nakamura K, Kubo A, Ichihara T. Ultra high resolution pinhole SPECT for small animal study. IEEE Trans Nucl Sci 1998;45:3122–6.
5. Hirai T, Nohara R, Ogoh S, Chen LG, Kataoka K, Li XH, et al. Serial evaluation of fatty acid metabolism in rats with myocardial infarction by pinhole SPECT. J Nucl Cardiol 2001;8:472–81.
6. Scherfler C, Donnemiller E, Schocke M, Dierkes K, Decristoforo C, Oberladstätter M, et al. Evaluation of striatal dopamine transporter function in rats by in vivo β-[^{125}I]CIT pinhole SPECT. Neuroimage 2002;17:128–41.
7. Acton PD, Choi SR, Plössl K, Kung HF. Quantification of dopamine transporters in the mouse brain using ultra-high resolution single-photon emission tomography. Eur J Nucl Med 2002;29:691–8.
8. Aoi T, Watabe H, Deloar HM, Ogawa M, Teramoto N, Kudomi N, et al. Absolute quantitation of regional myocardial blood flow of rats using dynamic pinhole SPECT. In: Conference Record of 2002 IEEE Nuclear Science Symposium and Medical Imaging Conference (CD-ROM). 2003. p. 1780–3.
9. Vanhove C, Defrise M, Franken PR, Everaert H, Deconinck F, Bossuyt A. Interest of the ordered subsets expectation maximization (OS-EM) algorithm in pinhole single-photon emission tomography reconstruction: a phantom study. Eur J Nucl Med 2000;27:140–6.
10. Shepp LA, Vardi Y. Maximum likelihood reconstruction for emission tomography. IEEE Trans Med Imag 1982;MI-1:113–22.
11. Hudson HM, Larkin RS. Accelerated image reconstruction using ordered subsets of projection data. IEEE Trans Med Imag 1994;13:601–9.
12. Feldkamp LA, Davis LC, Kress JW. Practical cone-beam algorithm. J Opt Soc Am A 1984;1:612–9.
13. Zeniya T, Watabe H, Aoi T, Kim KM, Teramoto N, Hayashi T, et al. A new reconstruction strategy for image improvement in pinhole SPECT. Eur J Nucl Med Mol Imaging 2004;31:1166–72.
14. Aoi T, Zeniya T, Watabe H, Deloar HM, Matsuda T, Iida H. System design and development of a pinhole SPECT system for quantitative functional imaging of small animals. Ann Nucl Med 2006;20:245–51.
15. Tuy HK. An inversion formula for cone-beam reconstruction. SIAM J Appl Math 1983;43:546–52.
16. Vollmar S, Michel C, Treffert JT, Newport DF, Casey M, Knöss C, et al. *HeinzelCluster*: accelerated reconstruction for FORE and OSEM3D. Phys Med Biol 2002;47:2651–8.

17. Shattuck DW, Rapela J, Asma E, Chatzioannou A, Qi J, Leahy RM. Internet2-based 3D PET image reconstruction using a PC cluster. Phys Med Biol 2002;47:2785–95.
18. Jones JP, Jones WF, Kehren F, Newport DF, Reed JH, Lenox MW, et al. SPMD cluster-based parallel 3-D OSEM. IEEE Trans Nucl Sci 2003;50:1498–502.
19. Jones JP, Jones WF, Everman J, Panin V, Michel C, Kehren F, et al. Impact of a high-performance communication network on cluster-based parallel iterative reconstruction. In: Conference Record of 2005 IEEE Nuclear Science Symposium and Medical Imaging Conference (CD-ROM), 2006. p. 2273–7.
20. Rong Z, Tianyu M, Yongjie J. Parallel OSEM reconstruction algorithm for fully 3-D SPECT on a Beowulf cluster. Conf Proc IEEE Eng Med Biol Soc 2005;2:1834–7.
21. Watabe H, Woo SK, Kim KM, Kudomi N, Iida H. Performance improvement of event-based motion correction for PET using a PC cluster. In: Conference Record of 2003 IEEE Nuclear Science Symposium and Medical Imaging Conference (CD-ROM), 2004. p. 2407–9.
22. Sohlberg A, Watabe H, Zeniya T, Iida H. Comparison of multi-ray and point-spread function based resolution recovery methods in pinhole SPECT reconstruction. Nucl Med Commun 2006;27:823–7.
23. Sohlberg A, Ruotsalainen U, Watabe H, Iida H, Kuikka JT. Accelerated median root prior reconstruction for pinhole single-photon emission tomography (SPET). Phys Med Biol 2003;48:1957–69.

Stroke

JOURNAL OF THE AMERICAN HEART ASSOCIATION

American Stroke Association℠

A Division of American Heart Association

Delayed Postischemic Treatment With Fluvastatin Improved Cognitive Impairment After Stroke in Rats

Munehisa Shimamura, Naoyuki Sato, Masataka Sata, Hitomi Kurinami, Daisuke Takeuchi, Kouji Wakayama, Takuya Hayashi, Hidehiro Iida and Ryuichi Morishita

Stroke published online Nov 1, 2007;
DOI: 10.1161/STROKEAHA.107.485045
Stroke is published by the American Heart Association. 7272 Greenville Avenue, Dallas, TX 72514
 Print ISSN: 0039-2499. Online ISSN: 1524-4628

Delayed Postischemic Treatment With Fluvastatin Improved Cognitive Impairment After Stroke in Rats

Munehisa Shimamura, MD, PhD; Naoyuki Sato, MD, PhD; Masataka Sata, MD, PhD; Hitomi Kurinami, MD; Daisuke Takeuchi, MD; Kouji Wakayama, MD; Takuya Hayashi, MD, PhD; Hidehiro Iida, MD, PhD; Ryuichi Morishita, MD, PhD

Background and Purposes—Recent clinical evidences indicate that statins may have beneficial effects on the functional recovery after ischemic stroke. However, the effect of delayed postischemic treatment with statins is still unclear. In the present study, we evaluated the effects of fluvastatin in the chronic stage of cerebral infarction in a rat model.

Methods—Rats exposed to permanent middle cerebral artery occlusion were treated for 3 months with fluvastatin beginning from 7 days after stroke. MRI, behavioral analysis, and immunohistochemistry were performed.

Results—Two months of treatment with fluvastatin showed the significant recovery in spatial learning without the decrease in serum total cholesterol level and worsening of infarction. Microangiography showed a significant increase in capillary density in the peri-infarct region in fluvastatin-treated rats after 3 months of treatment. Consistently, BrdU/CD31-positive cells were significantly increased in fluvastatin-treated rats after 7 days of treatment. MAP1B-positive neurites were also increased in the peri-infarct region in fluvastatin-treated rats. In addition, rats treated with fluvastatin showed the reduction of superoxide anion after 7 days of treatment and the reduction of Aβ deposits in the thalamic nuclei after 3 months of treatment.

Conclusions—Thus, delayed postischemic administration of fluvastatin had beneficial effects on the recovery of cognitive function without affecting the infarction size after ischemic stroke. Pleiotropic effects of fluvastatin, such as angiogenesis, neuritogenesis, and inhibition of superoxide production and Aβ deposition, might be associated with a favorable outcome. (***Stroke*. 2007;38:000-000.)**

Key Words: angiogenesis ■ cerebral infarct ■ microcirculation ■ statins

Despite conflicting data correlating cholesterol level with stroke, 2 early trials of HMG-CoA reductase inhibitors (statins) in patients after myocardial infarction patients showed a reduction in stroke risk as a secondary end point.[1] A meta-analysis of 9 statin intervention trials, which enrolled patients with coronary artery disease or those at high risk for coronary disease, demonstrated a 21% relative risk reduction for stroke after 5 years of treatment.[2] Another clinical evidence suggests that the commencement of statins within 4 weeks of a stroke results in a favorable 90-day outcome.[3] To clarify the effects of postischemic statin treatment, previous studies in which atorvastatin was started 1 day after stroke in rodents showed improvement of sensory motor deficit through induction of angiogenesis, neurogenesis, and synaptogenesis.[4,5] These pleiotropic effects of statins were shown to be the result of induction of vascular endothelial growth factor or brain-derived neurotrophic factor.[4] Additionally, the microvascular dysfunction in the posttreatment of stroke with recombinant human tissue-type plasminogen activator could be reduced by statins in rodent model.[6] However, the effect of delayed treatment with statins after ischemic stroke is still unknown. From this viewpoint, we investigated whether chronic statin treatment beginning 7 days after ischemic stroke had influences on neurological deficits and pathophysiology after the permanent middle cerebral artery occlusion (MCAo) model in rats.

Materials and Methods

Surgical Procedure

Male Wistar rats (270 to 300 grams; Charles River; Kanagawa, Japan) were used in this study. The right MCA was occluded by placement of poly-L-lysine–coated 4-0 nylon, as described previously.[7]

Protocol for Treatment and Behavioral Tests

Ten rats were only anesthetized (sham operation) and 32 rats were subjected to MCAo (day 1). Based on neuromuscular function on day 7, the rats were divided equally into saline-treated (n=16) or fluvastatin-treated (n=16) groups. Fluvastatin (5 mg/kg per day;

Received February 14, 2007; final revision received April 27, 2007; accepted May 30, 2007.

From Department of Advanced Clinical Science and Therapeutics (M.S., M.Sata, K.W.), Graduate School of Medicine, the University of Tokyo, Japan; Department of Clinical Gene Therapy (N.S., H.K., D.T., R.M.), Graduate School of Medicine, Osaka University, Japan; Department of Investigative Radiology (T.H., H.I.), National Cardiovascular Center, Research Institute, Japan.

Correspondence to Ryuichi Morishita, MD, PhD, Professor, Division of Clinical Gene Therapy, Graduate School of Medicine, Osaka University, 2-2 Yamada-oka, Suita 565-0871, Japan. E-mail morishit@cgt.med.osaka-u.ac.jp

Stroke is available at http://stroke.ahajournals.org

DOI: 10.1161/STROKEAHA.107.485045

provided by Novartis Pharma) or saline was given by gavage from day 7 to 100. We chose the dose (5 mg/kg per day), because a previous report showed that this dose could effectively induce angiogenesis in ischemic limb.[8] On day 55, neuromuscular function and locomotor activity were evaluated in the surviving rats. Then, cognitive function was examined by Morris water maze from day 56 to 63, because the effects of neuronal regeneration could be detected not in the early stage but in the chronic stage of ischemic brain such as 49 to 53 days after the insult.[9] On day 96, MRI was performed. On day 100, microangiography was performed.

MRI

High-resolution T1-weighted fast spin echo sequence images (repetition time [TR]=1500 ms; echo time [TE]=10.3 ms; field of view [FOV]=4× 3 cm; matrix=256×192; slice thickness=1.5 mm; slice gap=0.5 mm; number of slices=16; number of excitation=10; total time=9.39 min) were obtained using a 3-T MRI scanner (Signa LX VAH/I; GE).

Sensory Motor Deficit and Locomotor Activity

Although there are various batteries for testing sensory motor deficit, we used a simple protocol.[10] For forelimb flexion, rats were held by the tail on a flat surface. Paralysis of the forelimbs was evaluated by the degree of left forelimb flexion. For torso twisting, rats were held by the tail on a flat surface. The degree of body rotation was checked. For lateral push, rats were pushed either left or right. Rats with right MCA occlusion showed weak or no resistance against a left push. For hind limb placement, one hind limb was removed from the surface. Rats with right MCA occlusion showed delayed or no replacement of the hind limb when it was removed from the surface.

Spontaneous activity was measured via the open field (0.69 m^2). We set the sensor, which also put beams on the field, at 30 cm above the field. The number of count, which is when the animal crosses the beam, was measured for 30 minutes.

Morris Water Maze Task

A cylindrical tank 1.5 m in diameter was filled with water (25°C), and a transparent platform 15 cm in diameter was placed at a fixed position in the center of 1 of the 4 quadrants (O'Hara & Co, Ltd). In the hidden platform trials, we performed the tests 4 times per day for 4 days. When the rat could not reach the platform, the latency was set at 60 sec. In the visible platform trials, the tests were performed 4 times per day for 4 days. The acquired data were averaged per day.

Evaluation of Capillary Density

Using a recently developed microangiographic technique,[11] capillary density and blood–brain barrier leakage were evaluated in the cerebral cortex after MCA occlusion. The area or length of vessels was analyzed with an angiogenesis image analyzer (version 1.0; Kurabo).

Immunohistochemical Study: Bromodeoxyuridine Labeling

To identify newly formed DNA, saline-treated (n=5) and fluvastatin-treated (n=5) rats received injections of bromodeoxyuridine (BrdU, 50 mg/kg; Sigma-Aldrich, Saint Louis, Mo) intraperitoneally starting on day 7 twice per day until day 13. Rats were euthanized on day 14. After the sections (8-μm thickness) was fixed in 10% formaldehyde/MeOH neutral buffer solution and blocked, they were incubated with mouse monoclonal anti-rat CD31 antibody (1:100; BD Biosciences; San Jose, Calif), goat polyclonal anti-doublecortin (anti-DCX; Santa Cruz) antibody (1:100; Santa Cruz, Calif), mouse monoclonal anti-NeuN antibody (1:1000; Chemicon, Temecula, Calif), or mouse monoclonal anti-MAP1B antibody (1:100; Sigma-Aldrich), followed by anti-mouse goat fluorescent antibody (1:1000 for NeuN and MAP1B, 1:400 for CD31, Alexa Flour 546, Molecular Probes; Eugene, Ore) or anti-goat donkey fluorescent antibody (1:1000 for DCX Alexa Fluor 546). For double immunostaining, these sections were fixed again and incubated in 2 N HCl at 37°C for 30 minutes. After blocking, they were incubated with rat monoclonal anti-BrdU antibody (1:200; Abcam, Cambridge, UK) followed by anti-rat goat fluorescent antibody (1:1000, Alexa Fluor 488). For immunohistochemical staining for Aβ, sections were pretreated for 30 minutes with hot (85°C) citrate buffer as described before.[12] Confocal images were acquired using an FV-300 (Olympus).

Table. Infarction Volume Calculated by MRI, Blood Pressure, and Serum Total Cholesterol

	Sham	MCAo+S	MCAo+F	*P*
Infarction volume in total rats (mm^3)	...	283.8±23.9	278.4±26.4	0.851
Type of infarction in Figure 1a (N of rats)				0.828
A	...	12	11	...
B	...	3	3	...
C	...	1	2	...
Infarction volume (mm^3) in type A rats	...	322.8±15.0	327.0±18.8	0.758
Systolic blood pressure (mm Hg) in type A rats				
Day 7	116.1±5.4	123.7±6.0	115.5±7.3	0.654
Day 56	146.5±4.7	148.3±2.7	136.1±5.2	0.132
Serum total cholesterol (mg/dl) in type A rats on day 56	85.9±5.6	75.3±3.5	73.5±2.7	0.949

Type A, low-intensity area seen in the dorsolateral and lateral portions of the neocortex and the entire caudate putamen; type B, low-intensity area seen in the dorsolateral and lateral portions of the neocortex and in part of the caudate putamen; type C, low-intensity area seen in part of the lateral neocortex and caudate putamen. MCAo+S, saline-treated rats after MCAo; MCAo+F, fluvastatin-treated rats after MCAo.

P, saline vs fluvastatin.

Quantitative Histological Analysis

To quantify the immunoreactivity for MAP1B and Aβ, the acquired image was analyzed by Image J (version 1.32; NIH).

Detection of Superoxide Anion in Brain Sections

Superoxide anion was detected on day 14 as described previously.[13] Because intact cortex showed red fluorescence, we calculated the ratio of fluorescence as follows: ratio of fluorescence=[fluorescence intensity in ischemic core or peri-infarct region]/[fluorescence intensity in intact region].

Statistical Analysis

All values are expressed as mean±SEM. To analyze the differences in the type of cerebral infarction, χ^2 test was performed. The latency, path length, and mean speed in Morris water maze and sensory motor deficits were analyzed by a 2-factor repeated-measure ANOVA. Post hoc analyses were performed, and the Scheffe test was applied to control the inflation in type I error. The value of the serum total cholesterol, the blood pressure, and the spontaneous activity was analyzed by Scheffe rules. The differences in the immunohistochemistry and the volume of infarction were assessed by Mann–Whitney *U* analyses. In all cases, $P<0.05$ was considered significant.

Results

Effects of Fluvastatin on Cognitive Impairment

To confirm the severity of cerebral infarction, all rats were examined by T1-weighted MRI after 89 days of treatment. Although the total volume of infarction calculated in T1-weighted images was not different between rats treated with

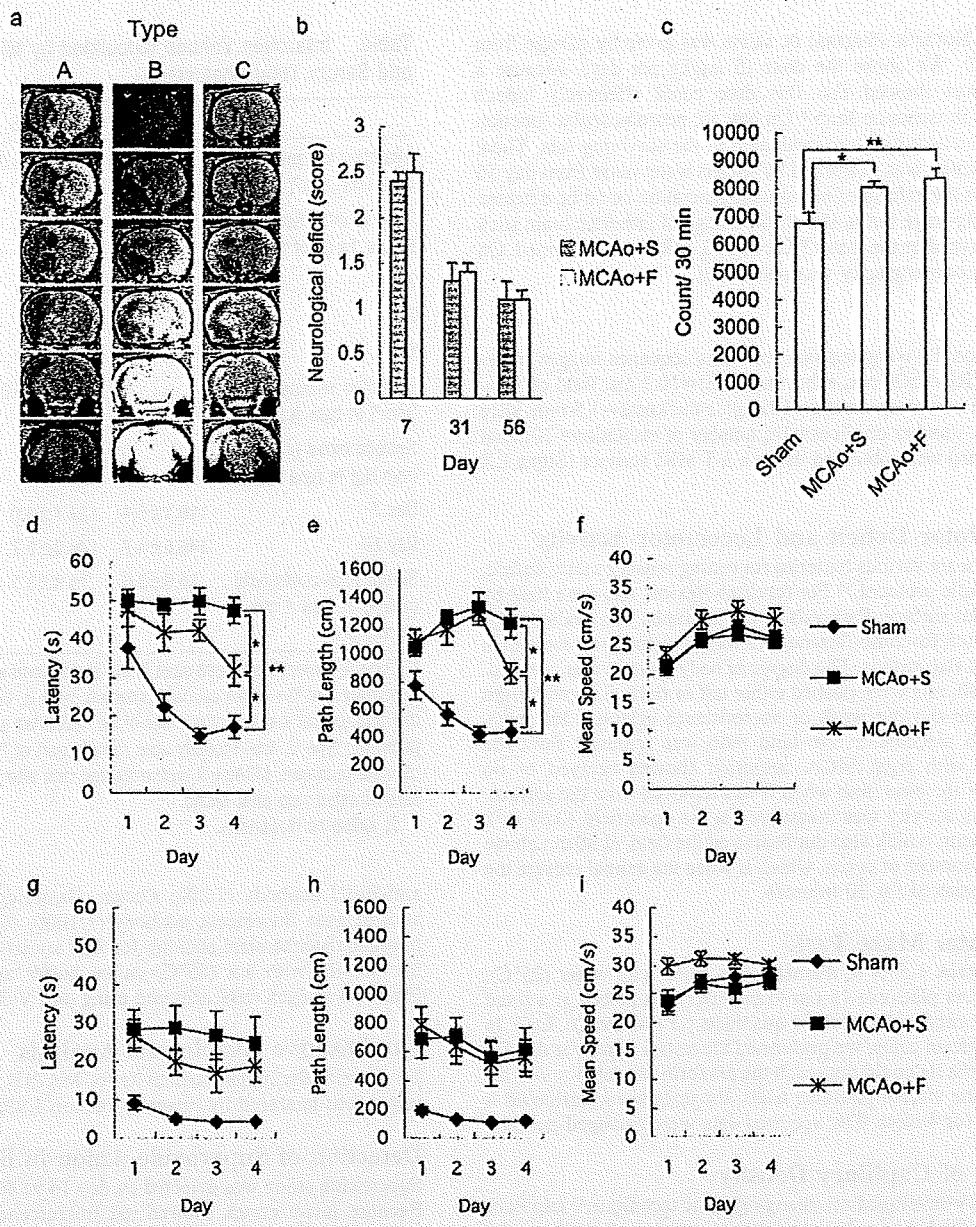

Figure 1. Typical T1-weighted image of coronal section of rat brain (a). The images were divided into 3 groups. Type A, low-intensity area seen in the dorsolateral and lateral portions of neocortex and the entire caudoputamen; type B, low-intensity area seen in the dorsolateral and lateral portions of neocortex and in part of the caudatoputamen; and type C, high-intensity area seen in part of the lateral neocortex and caudatoputamen. Sensory motor deficit (b). Spontaneous locomotor activity (c). Hidden platform test in Morris water maze. Each figure showed latency (d), path length (e), and mean speed (f). Days 1 to 4 indicate the trial day in the hidden platform test (56 to 59 days after middle cerebral artery occlusion). Visible platform test in Morris water maze. Each figure showed latency (g), path length (h), and mean speed (i). Days 1 to 4 indicate the day in the visible platform test (60 to 63 days after middle cerebral artery occlusion). MCAo+S indicates rats treated with saline after middle cerebral artery occlusion; MCAo+F, rats treated with fluvastatin after middle cerebral artery occlusion.

saline and fluvastatin (Table), the pattern of cerebral infarction was divided into 3 groups: type A, low-intensity area seen in the dorsolateral and lateral portions of the neocortex and the entire caudate putamen; type B, low-intensity area seen in the dorsolateral and lateral portions of the neocortex and in part of the caudate putamen; type C, low-intensity area seen in part of the lateral neocortex and caudate putamen (Figure 1a). In type C, most of the lateral neocortex was intact. To exclude the influence of the pattern of cerebral infarction on cognitive function, we focused on type A rats in the present study. The volume of cerebral infarction in type A rats was not different between the groups (Table). Blood pressure and serum total cholesterol also showed no difference among the groups (Table).

Sensory motor deficit had spontaneously recovered to some extent by 8 weeks in both groups, and there was no difference (Figure 1b). Locomotor activity in rats subjected to MCAo was increased as compared with that in sham-operated rats, as described before,[14] but there was no significant difference between fluvastatin-treated and saline-treated rats (Figure 1c). In Morris water maze (Figure 1d-i), which examines spatial learning, there were significant differences

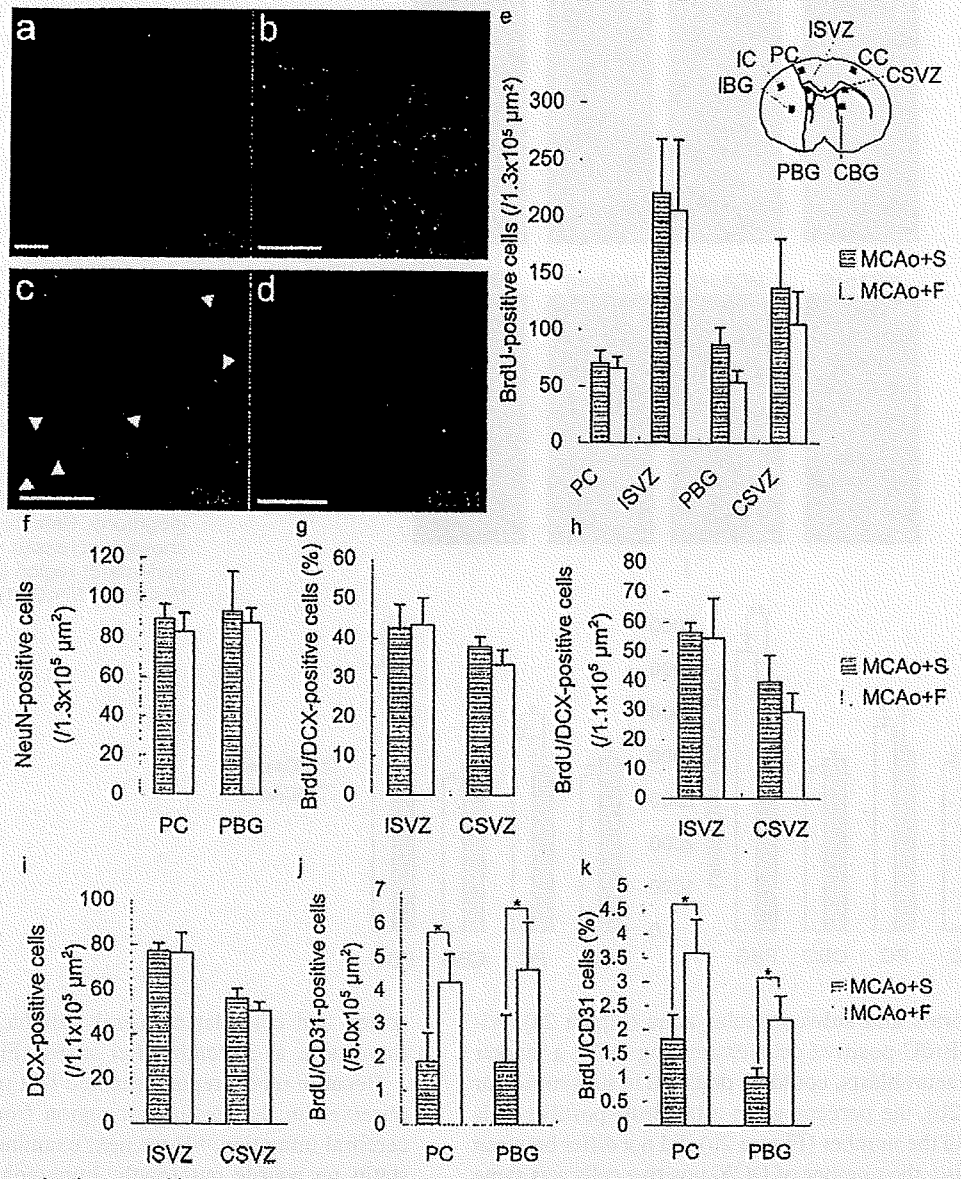

Figure 2. Representative images of immunohistochemical staining on day 14. Rats treated with fluvastatin (a through c), rats treated with saline (d). Although BrdU-positive cells were observed in the peri-infarct cortex (a), peri-infarct basal ganglia, and subventricular zone, these cells did not express NeuN (a), but expressed DCX in the subventricular zone (b). Fluvastatin-treated rats showed some BrdU/CD31-positive cells (arrows, c), although most BrdU-positive cells were negative for CD31 in saline-treated rats (d). The number of BrdU-positive cells (e), NeuN-positive cells (f), BrdU/DCX-positive cells (h), DCX-positive cells (i), and BrdU/CD31-positive cells (j); the percentage of BrdU/DCX-positive cells (g) or BrdU/CD31 cells (k) in total BrdU-positive cells. PC indicates peri-infarct cortex; PBG, peri-infarct basal ganglia; IC, infarcted cortex; IBG, ischemic basal ganglia; ISVZ, subventricular zone on infarcted side; CC, contralateral cortex, CSVZ, subventricular zone on contralateral side; CBG, contralateral basal ganglia (n=5 in each group, $^*P<0.05$, bar=100 μm).

in the latency and path length in hidden platform test among the groups (supplemental Table I, available online at http://stroke.ahajournals.org). A significant difference was observed on day 4 between fluvastatin-treated and saline-treated rats (supplemental Table I). Also, there was a significant difference between sham and saline-treated rats (supplemental Table I). There was no significant difference both in swimming speed and visible platform test, which excluded the possible influence of visual loss, sensory motor deficit, and motivation on the results.[15] These data suggest that impaired spatial learning was improved by fluvastatin.

Histological Changes by Fluvastatin

Next, we studied whether fluvastatin had some influences on the histology. Initially, we focused on neurogenesis and angiogenesis. To examine neurogenesis, we measured BrdU-incorporated cells after injecting BrdU from day 7 to day 13. Although BrdU-positive cells were observed in the subventricular zone and peri-infarct region (Figure 2a to 2d), the total number did not differ between the groups (Figure 2e). Similarly, the density of NeuN-positive cells, as a marker of adult neurons, also did not differ between the groups (Figure 2f), whereas there were no BrdU/NeuN-positive cells in the

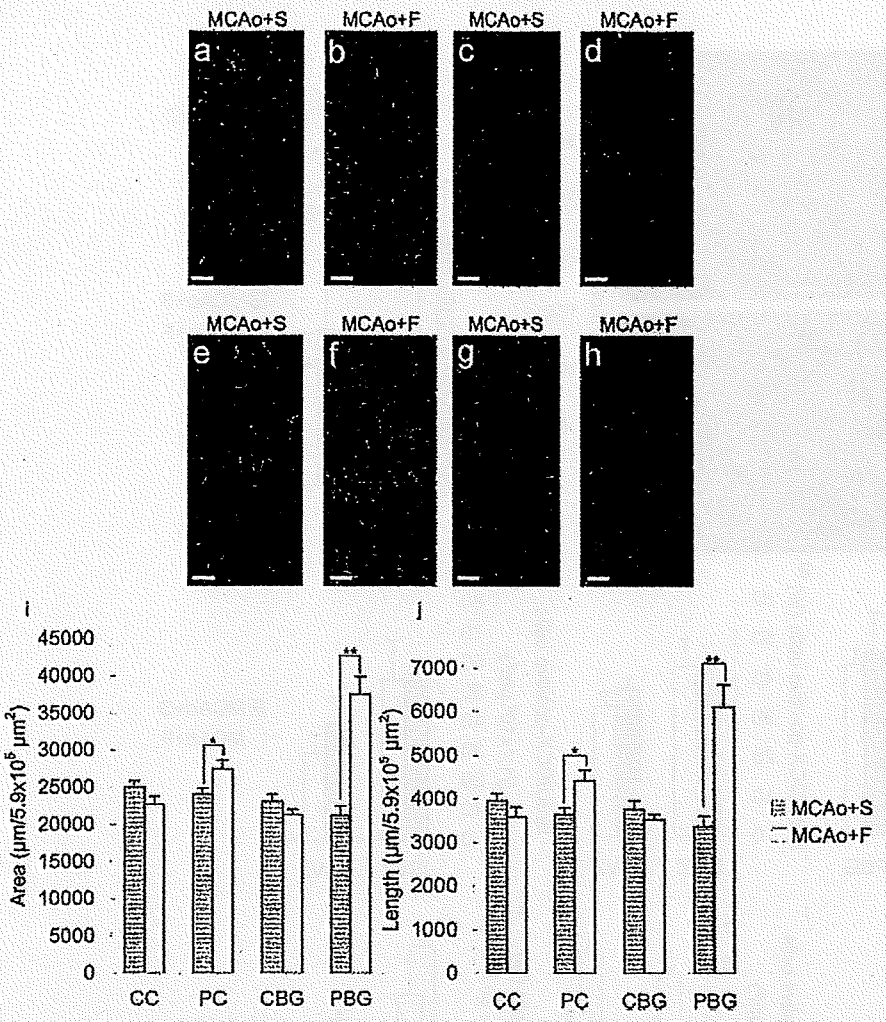

Figure 3. Microangiographic images using albumin-fluorescence isothiocyanate on day 100: (a and b) peri-infarct cortex; (c and d) contralateral cortex; (e and f) peri-infarct basal ganglia; (g and h) contralateral basal ganglia (bar=100 μm). Quantitative analysis (i and j) of microangiography. Rats treated with fluvastatin showed increased microvessels in the peri-infarct region (n=4 in each group, $^{*}P<0.05$, $^{**}P<0.01$).

peri-infarct cortex and subventricular zone (Figure 2a). Although some BrdU-positive cells expressing DCX, a marker for migrating neuroblasts, could be detected in subventricular zone (Figure 2b), the percentage in total BrdU-positive cells (Figure 2g) and the number (Figure 2h) did not differ between the groups. Also, the number of DCX-positive cells was same in the both groups (Figure 2i). There were no BrdU-positive cells expressing DCX in the cerebral cortex. Unexpectedly, these data suggest that neurogenesis was not enhanced by fluvastatin.

Thus, we further examined whether angiogenesis was affected by fluvastatin. In the peri-infarct cortex and basal ganglia, BrdU-positive cells that were positive for CD31 as a marker of endothelial cells could be detected (Figure 2c,2d). The number of BrdU/CD31-double-positive cells was significantly increased in fluvastatin-treated rats (Figure 2j). The percentage of BrdU/CD31-double-positive cells in total BrdU-positive cells was also increased in fluvastatin-treated rats (Figure 2k). Consistently, microangiography using FITC-conjugated albumin[11] also showed that microvessels were significantly increased in fluvastatin-treated rats only in the peri-infarct cortex and basal ganglia, without destruction of the blood–brain (Figure 3a to 3h). Quantitative analysis showed that the length and area of microvessels were also increased in the peri-infarct region, but not in the contralateral cortex and contralateral basal ganglia, in rats treated with fluvastatin, at 3 months after stroke (Figure 3i,j).

Because recent reports showed that neurite outgrowth was observed in the peri-infarct region from 7 to 14 days after cerebral infarction,[16,17] we next examined the effect of fluvastatin on neurite outgrowth. Immunohistochemical staining showed that treatment with fluvastatin significantly increased the immunoreactivity of MAP1B, a marker of neurite outgrowth, in neurites[16,18] (Figure 4), although the number of MAP1B-positive cells was the same in both groups. These data implied that the fluvastatin might promote angiogenesis, resulting in improvement of the microcirculation, and neurite outgrowth.

One possible explanation for the enhanced angiogenesis and neurite outgrowth is a decrease in oxidative stress by fluvastatin. To assess oxidative stress, we evaluated superoxide production using dihydroethidium staining (Figure 5a to 5e). Superoxide anion was increased in the ischemic core as compared with the contralateral region at 2 weeks after MCA occlusion (Figure 5a,5c). However, rats treated with fluvastatin showed a significant reduction in superoxide anion especially in the ischemic core region, but not in the peri-infarct cortex and basal ganglia (Figure 5b,5d,5e).

Finally, we examined Aβ deposition in the thalamic nuclei, because previous reports showed that Aβ deposits in the

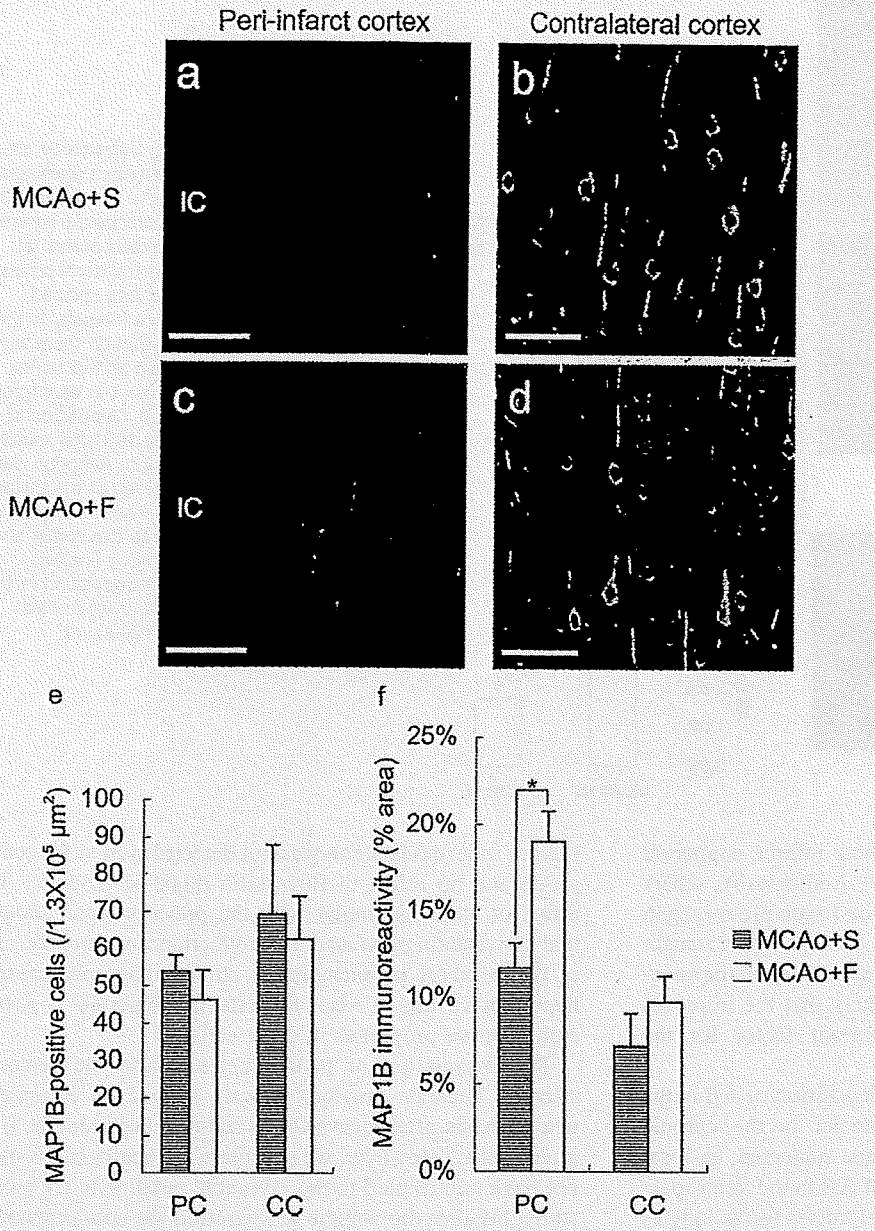

Figure 4. Typical images of immunohistochemical staining for MAP1B in peri-infarct cortex (a and c) and contralateral cortex (b and d) on day 14 (bar=100 μm). Although the number of MAP1B-positive cells was the same in both groups (e), immunoreactivity was higher in the peri-infarct region in fluvastatin-treated rats (f) (n=4 in each group, *P<0.05).

thalamic nuclei persisted as long as 9 months after focal cerebral ischemia.[12] Although immunohistochemical staining showed marked deposition of Aβ in the ventrolateral and ventromedial thalamic nuclei at 3 months after stroke, the area of Aβ deposits was significantly decreased in fluvastatin-treated rats (Figure 5f to 5h). In other regions, such as cortex or basal ganglia, there was no Aβ deposits in both groups as reported before.[12]

Discussion

Although several laboratories have shown that long-term pretreatment with a statin reduces infarct size in rodents,[19] no articles have reported the effects of delayed postischemic treatment with statins. The present study demonstrated that statin treatment beginning 7 days after ischemic stroke resulted in significant improvement of spatial learning at 8 weeks after stroke, without any change in the plasma cholesterol level and infarct size.

Fluvastatin-treated rats showed a significant increase of MAP1B in neurites in the peri-infarct region. Considering that MAP1B is especially prominent in extending neurites[20] and related to functional recovery after ischemic stroke,[17] one of the possible effects of fluvastatin is to enhance neurite outgrowth, "neuritogenesis," in the early stage of treatment. This speculation might be supported by the recent study demonstrating that neurite outgrowth is accelerated by pravastatin via inhibiting the activity of geranylgeranylated proteins such as RhoA.[21]

As BrdU/CD31-positive cells were increased 14 days after MCAo and microvessels were also increased in the peri-infarct region 100 days after MCAo, fluvastatin enhanced angiogenesis and resulted in improvement of microcirculation in the peri-infarct region. Although the relationship between the improved microcirculation and behavior is still unclear, a recent report demonstrated that the restoration of perfusion by collateral growth and new capillaries in the

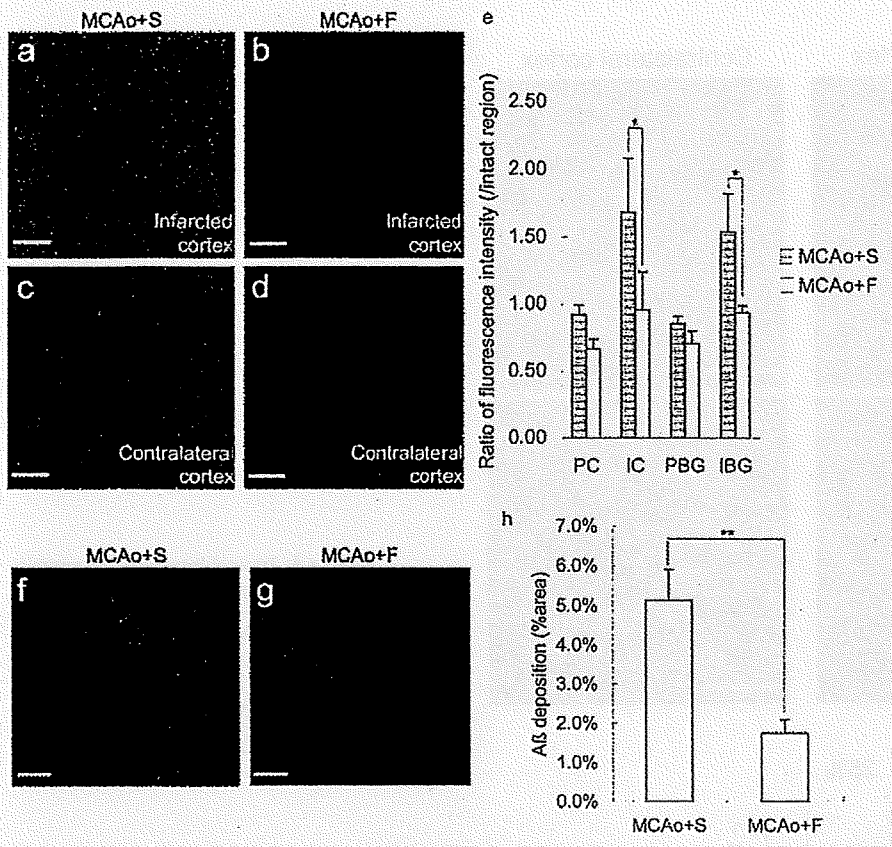

Figure 5. a through e, Superoxide anion detected by dihydroethidium staining on day 14. Red spots show the existence of superoxide anion. Fluorescence intensity was higher in the infarcted cortex (a) compared with the contralateral cortex (c). Fluvastatin-treated rats showed decreased fluorescence intensity in the infarcted cortex (b), although there was no difference in the peri-infarct cortex and basal ganglia (e) (n=4 in each group, $^{*}P<0.05$, bar=100 μm). Deposition of Aβ in thalamus on day 100 after middle cerebral artery occlusion. Although deposition of Aβ was observed in the thalamic nuclei (f and g), there was no deposition in other regions such as the cortex and basal ganglia. Quantitative analysis showed decreased Aβ deposition in fluvastatin-treated rats (h) (n=6 in each group, $^{**}P<0.01$, bar=200 μm).

ischemic border zone around a cortical infarct supported long-term functional recovery in rats.[22] Additionally, others reported that some patients who received tissue plasminogen activator therapy with no immediate clinical improvement despite early recanalization showed delayed clinical improvement.[23] From these viewpoints, it is likely that the improvement of microcirculation is an important factor for the functional recovery.

Of importance, fluvastatin reduced deposition of Aβ in the ventrolateral–ventromedial thalamic nuclei in the chronic stage of ischemic stroke, although rats subjected to focal cerebral ischemia develop deposition of Aβ in the ventroposterior lateral and ventroposterior medial nuclei for as long as 9 months.[12] This might be similar with precious reports showing that statins reduced the production of Aβ in Alzheimer disease.[24] The mechanism of the reduction of Aβ by fluvastatin should be further investigated.

Thus, the rats treated with fluvastatin showed enhancement of angiogenesis and neurite outgrowth in the peri-infarct cortex and reduced deposition of Aβ in the ventrolateral–ventromedial thalamic nuclei. Because those regions are important sites for spatial learning,[25,26] we speculate that the enhancement of functional recovery by fluvastatin might be dependent on those regions.

The other histological difference was the reduction of superoxide anion in the ischemic core in fluvastatin-treated rats. Because cerebral blood flow in the ischemic cortex remained to be reduced for 48 hours and restored to some extent 9 days after permanent MCAo,[27] we speculate that fluvastatin could reach the ischemic core and show the antioxidative effects. On the contrary, in the peri-infarct region, superoxide anion was not detected even in the control group and no effect of fluvastatin might be observed. This effect of statin is similar with the previous report showing that cerivastatin prevented the production of superoxide anion in the cerebral parenchyma in stroke-prone spontaneously hypertensive rats.[28] Also, fluvastatin is reported to possess antioxidative properties in other cells.[29,30]

The association of neurogenesis is also the center of interest, because previous reports showed an increase in neurogenesis after atorvastatin treatment beginning at 1 day after stroke.[5] However, we speculate that neurogenesis might not have contributed to the favorable outcome in the present study, because the volume of infarction was not decreased by fluvastatin, and the density of mature neurons (NeuN-positive cells) and proliferative immature neurons (BrdU/DCX-positive cells) was the same in both groups. From the viewpoints, the timing of treatment seems important for the enhancement of neurogenesis and the beginning of statin 7 days after MCAo might be too late to enhance neurogenesis.

The limitation of the present study is that there is no data demonstrating that fluvastatin crossed over the blood–brain barrier and acted on neurons directly. Blood–brain barrier permeability differs among statins and correlates in part with their respective lipophilicity.[31] Considering that pretreatment with pravastatin and rosuvastatin, whose lipophilicity is 0.84 and 0.33, respectively, shows significant effects on reducing infarction volume,[31] fluvastatin, whose lipophilicity is 1.27, might penetrate blood–brain barrier and have some direct effects on neurons. Otherwise, fluvastatin could penetrate the brain because of the disruption of blood–brain barrier after MCAo. One of other limitations in the present study is no

examination of the characteristics of BrdU positive-cells other than CD31, DCX, or NeuN. In addition, how these histological changes in fluvastatin-treated rats were mechanistically linked to improved outcome was not clarified. Further study is necessary to clarify these points.

Summary

Overall, delayed postischemic chronic fluvastatin treatment showed beneficial effects on the recovery of cognitive impairment after stroke by enhancement of neuritogenesis and of angiogenesis and a decrease in Aβ deposition and superoxide anion production. Further studies might show potential clinical utility to treat cognitive impairment in patients with ischemic stroke.

Acknowledgments

The authors thank Dr Masatsugu Horiuchi and Dr Masaru Iwai for their helpful advice on superoxide detection by dihydroethidium staining, and Dr Hiroshi Sato for assistance with MRI.

Sources of Funding

This work was partially supported by a Grant-in-Aid from the Organization for Pharmaceutical Safety and Research, a Grant-in-Aid from The Ministry of Public Health and Welfare, a Grant-in-Aid from Japan Promotion of Science, and a Grant-in-Aid from the Ministry of Education, Culture, Sports, Science, and Technology, of the Japanese Government.

Disclosures

Fluvastatin was donated from Novartis Pharma. Masataka Sata received Honoraria payment (modest) from Novartis Pharma. Ryuichi Morishita received honoraria payment (modest) and has an advisory board relationship to Novartis Pharma.

References

1. Sacks FM, Pfeffer MA, Moye LA, Rouleau JL, Rutherford JD, Cole TG, Brown L, Warnica JW, Arnold JM, Wun CC, Davis BR, Braunwald E. The effect of pravastatin on coronary events after myocardial infarction in patients with average cholesterol levels: cholesterol and recurrent events trial investigators. *N Engl J Med.* 1996;335:1001–1009.
2. Amarenco P, Tonkin AM. Statins for stroke prevention: disappointment and hope. *Circulation.* 2004;109:III44–49.
3. Moonis M, Kane K, Schwiderski U, Sandage BW, Fisher M. HMG-CoA reductase inhibitors improve acute ischemic stroke outcome. *Stroke.* 2005;36:1298–1300.
4. Chen J, Zhang C, Jiang H, Li Y, Zhang L, Robin A, Katakowski M, Lu M, Chopp M. Atorvastatin induction of VEGF and BDNF promotes brain plasticity after stroke in mice. *J Cereb Blood Flow Metab.* 2005;25: 281–290.
5. Chen J, Zhang ZG, Li Y, Wang Y, Wang L, Jiang H, Zhang C, Lu M, Katakowski M, Feldkamp CS, Chopp M. Statins induce angiogenesis, neurogenesis, and synaptogenesis after stroke. *Ann Neurol.* 2003;53: 743–751.
6. Zhang L, Zhang ZG, Ding GL, Jiang Q, Liu X, Meng H, Hozeska A, Zhang C, Li L, Morris D, Zhang RL, Lu M, Chopp M. Multitargeted effects of statin-enhanced thrombolytic therapy for stroke with recombinant human tissue-type plasminogen activator in the rat. *Circulation.* 2005;112:3486–3494.
7. Belayev L, Alonso OF, Busto R, Zhao W, Ginsberg MD. Middle cerebral artery occlusion in the rat by intraluminal suture: neurological and pathological evaluation of an improved model. *Stroke.* 1996;27:1616–1623.
8. Sata M, Nishimatsu H, Osuga J, Tanaka K, Ishizaka N, Ishibashi S, Hirata Y, Nagai R. Statins augment collateral growth in response to ischemia but they do not promote cancer and atherosclerosis. *Hypertension.* 2004;43: 1214–1220.
9. Nakatomi H, Kuriu T, Okabe S, Yamamoto S, Hatano O, Kawahara N, Tamura A, Kirino T, Nakafuku M. Regeneration of hippocampal pyramidal neurons after ischemic brain injury by recruitment of endogenous neural progenitors. *Cell.* 2002;110:429–441.
10. Petullo D, Masonic K, Lincoln C, Wibberley L, Teliska M, Yao DL. Model development and behavioral assessment of focal cerebral ischemia in rats. *Life Sci.* 1999;64:1099–1108.
11. Cavaglia M, Dombrowski SM, Drazba J, Vasanji A, Bokesch PM, Janigro D. Regional variation in brain capillary density and vascular response to ischemia. *Brain Res.* 2001;910:81–93.
12. van Groen T, Puurunen K, Maki HM, Sivenius J, Jolkkonen J. Transformation of diffuse beta-amyloid precursor protein and beta-amyloid deposits to plaques in the thalamus after transient occlusion of the middle cerebral artery in rats. *Stroke.* 2005;36:1551–1556.
13. Iwai M, Liu HW, Chen R, Ide A, Okamoto S, Hata R, Sakanaka M, Shiuchi T, Horiuchi M. Possible inhibition of focal cerebral ischemia by angiotensin II type 2 receptor stimulation. *Circulation.* 2004;110: 843–848.
14. Robinson RG. Differential behavioral and biochemical effects of right and left hemispheric cerebral infarction in the rat. *Science.* 1979;205: 707–710.
15. DeVries AC, Nelson RJ, Traystman RJ, Hurn PD. Cognitive and behavioral assessment in experimental stroke research: Will it prove useful? *Neurosci Biobehav Rev.* 2001;25:325–342.
16. Badan I, Platt D, Kessler C, Popa-Wagner A. Temporal dynamics of degenerative and regenerative events associated with cerebral ischemia in aged rats. *Gerontology.* 2003;49:356–365.
17. Badan I, Dinca I, Buchhold B, Suofu Y, Walker L, Gratz M, Platt D, Kessler CH, Popa-Wagner A. Accelerated accumulation of n- and c-terminal beta app fragments and delayed recovery of microtubule-associated protein 1b expression following stroke in aged rats. *Eur J Neurosci.* 2004;19:2270–2280.
18. Schabitz WR, Berger C, Kollmar R, Seitz M, Tanay E, Kiessling M, Schwab S, Sommer C. Effect of brain-derived neurotrophic factor treatment and forced arm use on functional motor recovery after small cortical ischemia. *Stroke.* 2004;35:992–997.
19. Endres M, Laufs U, Liao JK, Moskowitz MA. Targeting enos for stroke protection. *Trends Neurosci.* 2004;27:283–289.
20. Gonzalez-Billault C, Avila J, Caceres A. Evidence for the role of map1b in axon formation. *Mol Biol Cell.* 2001;12:2087–2098.
21. Pooler AM, Xi SC, Wurtman RJ. The 3-hydroxy-3-methylglutaryl co-enzyme a reductase inhibitor pravastatin enhances neurite outgrowth in hippocampal neurons. *J Neurochem.* 2006;97:716–723.
22. Wei L, Erinjeri JP, Rovainen CM, Woolsey TA. Collateral growth and angiogenesis around cortical stroke. *Stroke.* 2001;32:2179–2184.
23. Alexandrov AV, Hall CE, Labiche LA, Wojner AW, Grotta JC. Ischemic stunning of the brain: Early recanalization without immediate clinical improvement in acute ischemic stroke. *Stroke.* 2004;35:449–452.
24. Fassbender K, Simons M, Bergmann C, Stroick M, Lutjohann D, Keller P, Runz H, Kuhl S, Bertsch T, von Bergmann K, Hennerici M, Beyreuther K, Hartmann T. Simvastatin strongly reduces levels of Alzheimer's disease beta -amyloid peptides Abeta 42 and Abeta 40 in vitro and in vivo. *Proc Natl Acad Sci U S A.* 2001;98:5856–5861.
25. Casu MA, Wong TP, De Koninck Y, Ribeiro-da-Silva A, Cuello AC. Aging causes a preferential loss of cholinergic innervation of characterized neocortical pyramidal neurons. *Cereb Cortex.* 2002;12:329–337.
26. Jeljeli M, Strazielle C, Caston J, Lalonde R. Effects of ventrolateral-ventromedial thalamic lesions on motor coordination and spatial orientation in rats. *Neurosci Res.* 2003;47:309–316.
27. Rudin M, Baumann D, Ekatodramis D, Stirnimann R, McAllister KH, Sauter A. MRI analysis of the changes in apparent water diffusion coefficient, t(2) relaxation time, and cerebral blood flow and volume in the temporal evolution of cerebral infarction following permanent middle cerebral artery occlusion in rats. *Exp Neurol.* 2001;169:56–63.
28. Kawashima S, Yamashita T, Miwa Y, Ozaki M, Namiki M, Hirase T, Inoue N, Hirata K, Yokoyama M. HMG-CoA reductase inhibitor has protective effects against stroke events in stroke-prone spontaneously hypertensive rats. *Stroke.* 2003;34:157–163.
29. Sumi D, Hayashi T, Thakur NK, Jayachandran M, Asai Y, Kano H, Matsui H, Iguchi A. A HMG-CoA reductase inhibitor possesses a potent anti-atherosclerotic effect other than serum lipid lowering effects–the relevance of endothelial nitric oxide synthase and superoxide anion scavenging action. *Atherosclerosis.* 2001;155:347–357.
30. Morita H, Saito Y, Ohashi N, Yoshikawa M, Katoh M, Ashida T, Kurihara H, Nakamura T, Kurabayashi M, Nagai R. Fluvastatin ameliorates the hyperhomocysteinemia-induced endothelial dysfunction: The antioxidative properties of fluvastatin. *Circ J.* 2005;69:475–480.
31. Endres M. Statins and stroke. *J Cereb Blood Flow Metab.* 2005;25: 1093–1110.

Table I. Statistics in Morris Water Maze

	Hidden Test			Visible Test		
	Latency	Length	Speed	Latency	Length	Speed
P values in 2-factor repeated-measure ANOVA (Sham, MCAo+S, MCAo+F)						
Treatment	<0.001	<0.001	0.053	0.004	0.021	0.342
Day	<0.001	0.011	<0.001	0.003	0.014	0.288
Treatment×Day	0.002	<0.001	0.855	0.465	0.684	0.306
P values in Scheffe test on day 4						
Sham vs MCAo+S	<0.001	<0.001	0.933	0.018	0.025	0.585
Sham vs MCAo+F	0.024	0.010	0.277	0.138	0.058	0.266
MCAo+S vs MCAo+F	0.012	0.023	0.129	0.643	0.941	0.820

MCAo+S indicates saline-treated rats after MCAo; MCAo+F, fluvastatin-treated rats after MCAo.

癌診断におけるPET/SPECT技術 —過去・現在・未来

渡部浩司

PETおよびSPECT技術は，現在，癌診断において大きな役割を担っている．PET/SPECT技術は，物理学，化学，薬学，生物学，医学，情報学など，さまざまな基礎分野の統合した技術であり，現在のPET/SPECTの発展は，個々の基礎研究の進歩のうえに成り立っている．本稿では，PET/SPECT技術をさまざまな視点から眺め，現在の，そして将来の癌診断におけるPET/SPECTの技術に関して概説する．

はじめに

2002年にFDG-PET（fluoro-2-deoxy-D- glucose-positron emission tomography）の健康保険の適用が開始され，"PET検診"という言葉がマスコミでも取り上げられるようになり，またたく間にPETが市民権を得るようになった．しかし，PET自身は，決して新しい技術ではなく，X線CTと同様の古い歴史をもっており，ゆっくりと成熟してきた技術といえる．PET/SPECTにかかわる技術は物理学，化学，薬学，生物学，医学，情報学など多岐に渡っており，それぞれの分野の基礎的な研究の成果が統合されて，今日のPET/SPECT技術がある．

PET/SPECTを用いた癌診断において検出能を上げるためには，以下のような因子が重要となる．

・感度
・空間分解能
・腫瘍選択性

これらの因子の上昇のために，さまざまなアプローチが行われてきた．本稿では，癌診断におけるPET/SPECT技術の過去，現在，そして未来に関して述べ，基礎技術研究がどのようにPET/SPECTに応用されているかを鳥瞰したい．

[キーワード&略語]
PET, SPECT, FDG, 腫瘍マーカー
PET：positron emission tomography（陽電子断層撮影法）
SPECT：single photon emission computed tomography（単一光子断層撮影法）
FDG：fluoro-2-deoxy-D-glucose（フルオロデオキシグルコース）
FBP法：filtered back-projection法（フィルタ付逆投影法）
OSEM法：ordered subset expectation maximaization法（サブセット化による期待値最大化法）
FORE法：fourier rebinning法
CAD：computer-aided diagnosis（コンピュータ自動診断）

Overview of PET and SPECT techniques for cancer diagnosis

Hiroshi Watabe：Department of Investigative Radiology, Advanced Medical Engineering Center, National Cardiovascular Center Research Institute（国立循環器病センター研究所先進医工学センター放射線医学部）